Spectroscopy and dynamics of methylamine. I. Rotational and vibrational structures of CH_3NH_2 and CH_3ND_2 in $\tilde{A}$ states

Sun Jong Baek, Kyo-Won Choi, and Young S. Choi
Department of Chemistry, Inha University, Incheon (402-751), Republic of Korea

Sang Kyu Kim[a)]
Department of Chemistry, Inha University, Incheon (402-751), Republic of Korea and Department of Chemistry and School of Molecular Sciences, Korea Advanced Institute of Science and Technology (KAIST), Daejeon (305-701), Republic of Korea

(Received 16 December 2002; accepted 27 March 2003)

Rovibrational structures of methylamines (CH_3NH_2 and CH_3ND_2) in predissociative $\tilde{A}$ states ($3s-n$) are investigated using (1+1) resonant-enhanced two-photon ionization (R2PI) spectroscopy. A part of experimental results was briefly reported earlier [J. Chem. Phys. **117**, 10057 (2002)], and full detailed results and analyses are given here. Spectral origins are determined to be 41 669 and 42 038 cm^{-1} for CH_3NH_2 and CH_3ND_2, respectively. Amino wagging and CH_3 rocking modes are optically active, giving their respective fundamental frequencies of 636 (487) and 1008 (1012) cm^{-1} for CH_3NH_2 (CH_3ND_2). The CH_3 moiety is found to rotate nearly freely about the C–N axis with respect to the amino group with an accurately determined torsional barrier of 5.0 ± 0.5 cm^{-1} at the zero-point level of $CH_3ND_2(\tilde{A})$. The torsional barrier increases to 19.0 ± 0.5 cm^{-1} at the v (ND_2-wag)=1 level due to wagging-torsional mode coupling. Both internal and overall rotational fine structures are clearly resolved for the first few vibrational levels of $CH_3ND_2(\tilde{A})$, providing accurate values of vibrational frequencies and associated internal and overall rotational constants. Broad spectral features of the CH_3NH_2 excitation spectrum are unambiguously assigned by using the internal rotor Hamiltonian established in the analysis of the CH_3ND_2 excitation spectrum. Linewidths of spectral bands provide lifetimes of corresponding quantum states excited at particular rovibrational levels, giving, for example, ~8.8 and ~1.8 ps for zero-point and v (ND_2-wag)=2 levels of the CH_3ND_2 ($\tilde{A}$) state, respectively. The lifetime of $CH_3NH_2(\tilde{A})$ is estimated to be much shorter, giving $\tau\sim0.38$ ps at the origin band. The large H/D isotope effect in lifetimes of excited states indicates that the primary dissociation channel is the N–H(D) bond dissociation and it proceeds via tunneling through a reaction barrier. Lifetimes are found to be mode specific, showing the experimental fact that energy deposition to a certain vibrational mode, which is perpendicular to the reaction coordinate, may modify the reaction barrier along the N–H(D) reaction coordinate. *Ab initio* results for structures and vibrational frequencies of methylamines at excited states are compared with the experiment. © *2003 American Institute of Physics.* [DOI: 10.1063/1.1575734]

I. INTRODUCTION

The spectroscopy and dynamics of primary amines are quite meaningful to investigate, since fundamental properties regarding the structures and reactivity of those molecules are essential in understanding the role of primary amines in many chemical reactions important in organic syntheses and biological processes. In 1963, Michael and Noyes[1] reported that the N–H bond dissociation is a dominant reaction channel with a yield of more than 75% from the first-excited methylamine dissociation, while other reactions such as C–H bond dissociation and H_2 formation channels are ~7.5% and less than 10%, respectively. More recently, sophisticated experiments on the photodissociation dynamics of CH_3NH_2 were carried out by several research groups.[2–7] The Butler group[4] measured translational energies of different products from several reaction channels of the CH_3NH_2 dissociation at 222 nm to conclude that the major channel is N–H bond dissociation while the C–H and C–N bond dissociation channels are also significant. On the other hand, the Ashfold group,[5,6] through H-atom Rydberg-tagged high-resolution translational spectroscopy, had reached a conclusion that the H fragment, slow and fast, is almost entirely from the N–H bond dissociation, suggesting that the C–H bond breakage practically does not occur. According to theoretical calculations by the Morokuma group[8] for the N–H bond fission, the first-excited state of methylamine has a 3*s* Rydberg character in the Franck–Condon region and it is immediately followed by coupling with a repulsive valence state correlating diabatically to the ground products. Similar to the N–H bond dissociation of ammonia,[9–15] the dissociative excited state crosses with the ground electronic state which diabatically correlates to excited products, $H+CH_3NH(\tilde{A})$, in the late

a)Author to whom correspondence should be addressed. Electronic mail: skkim@inha.ac.kr

stage along the N–H reaction coordinate. Even though these earlier studies[2–7] provide very important insights into potential energy surfaces on which many different reactions take place, state-to-state reaction dynamic studies, which are extremely useful, had not been plausible especially since initial reactant states have been poorly characterized until very recently.

Methylamine is the simplest primary amine, and thus its rovibrational structure has been thoroughly studied for the ground electronic state using microwave and/or far-infrared spectroscopy.[16–23] However, for the first-excited state of methylamine, assignments for the spectral origin and associated vibrational bands had been in dispute for quite a long time. Absorption spectra of methylamine in the gas phase at room temperature had been taken by a number of groups.[24–29] The first UV spectrum of methylamine was reported by Föster and Jungers in 1937.[24] They determined the 0–0 transition energy to be 41 680 cm^{-1} and found that two vibrational modes with frequencies of 650 and 1000 cm^{-1} are optically active, of which the former is associated with the amino moiety while the latter is more likely associated with the methyl group. In the more extended work reported in 1953 by Tannenbaum *et al.*,[25] the 0–0 transition was reported to be 41 690 cm^{-1} and vibrational bands with fundamental frequencies of 660 and 1000 cm^{-1} were claimed to be due to N–H bending and C–N stretching, respectively. Later, Tsuboi *et al.*[26,27] located the origin of CH_3NH_2 at 41 715 cm^{-1} and assigned 651 and 1004 cm^{-1} bands as NH_2 wagging and CH_3 rocking modes, respectively. More recently, Taylor *et al.*[28,29] reported the first mass-resolved excitation spectra of supersonically cooled methylamine and its isotopomers. Comparing their experimental results with *ab initio* calculation, Taylor *et al.* concluded that the spectral origin is not observed in the experiment due to a severe geometrical change occurring upon electronic excitation. Accordingly, they claimed that the CH_3NH_2 origin is expected to be located at 39 770 cm^{-1} and optically active modes are amino wagging and scissoring with frequencies of 642 and 1476 cm^{-1}, respectively.[28] The disagreement continued in a methylamine UV–VUV high-resolution absorption study reported by Hubin-Franskin *et al.* in 2002.[30] According to them, the CH_3NH_2 origin is at 41 771 cm^{-1} and bands located at 637, 984, and 371 cm^{-1} above the origin are NH_2 wagging, C–N stretching, and two quanta of NH_2 torsion, respectively. These confusing disagreements, which continued for the past 65 years among previous experimental works for excited methylamine spectroscopy, are partly related to broad spectral features of the CH_3NH_2 excitation spectrum.

Very recently, our group has reported the (1+1) resonant-enhanced two-photon ionization (R2PI) spectra of jet-cooled CH_3NH_2 and CH_3ND_2, finding that spectral broadening is actually due to the ultrashort lifetimes of predissociating $\tilde{A}$ states.[31] Because of the relatively longer lifetimes of CH_3ND_2 excited states, its rotational fine structures could be revealed. And it was found that the CH_3 group nearly freely rotates with respect to the amino moiety in the excited state. It should be noted that in 1982 Tsuboi and Yirakawa[27] reported a preliminary analysis of the rotational structure of the CH_3ND_2 origin absorption band taken in the gas phase at room temperature, in which they also concluded the internal free rotation of CH_3 with respect to ND_2 with a torsional barrier less than 1 cm^{-1}. In our earlier report, a Hamiltonian for free internal rotation was also quite useful in interpreting the CH_3NH_2 spectrum nicely, giving confirmative assignments for vibational bands in the excitation spectrum.[31] Accordingly, spectral assignments were firmly established giving the 0–0 transition energy of 41 669 cm^{-1} for the first-excited CH_3NH_2.[31] Optically active modes are NH_2 wagging and CH_3 rocking modes with their respective fundamental frequencies of 636 and 1008 cm^{-1}. It is interesting to note that accurately determined spectroscopic values are closer to those reported 65 years ago than more recently reported values.

In this work, full detailed analyses of excitation spectra of CH_3NH_2 and CH_3ND_2 are given. Much richer information about the excited methylamine structure is presented here compared to the earlier brief publication.[31] An internal-rotor Hamiltonian including a torsional barrier is employed for the perfect match of experiment and theory. Torsional barriers are thus both precisely and accurately determined for the first few vibrational bands in the CH_3ND_2 excitation spectrum. Vibrational frequencies and associated internal and overall rotational constants are accurately determined to give a quantitative description of potential energy surfaces of CH_3NH_2 and CH_3ND_2 in their $\tilde{A}$ states. Lifetimes are deduced for all vibronic bands, giving energy- and mode-dependent predissociation rates in excited states of CH_3NH_2 and CH_3ND_2. A plausible predissociation mechanism is also discussed in comparison with previously reported dynamics studies.

II. EXPERIMENT

The methylamine sample (CH_3NH_2, Aldrich) was purchased and used without further purification. As described in the earlier publication,[31] CH_3ND_2 was synthesized by repeating the process of the CH_3NH_2 dissolution in D_2O followed by dehydration in KOH solution. Methylamine samples were introduced into gas cylinders to prepare 2% of methylamine gases (CH_3NH_2 or CH_3ND_2) in neon gas. The gas mixture was then expanded through a 0.3-mm-diam nozzle orifice (General Valve) into a differentially pumped molecular beam chamber equipped with two turbo-molecular pumps. The backing pressure was ~3.5 atm, and the repetition rate was 10 Hz. The molecular beam was skimmed through a 1-mm-diam skimmer (Precision Instrument Services). Background pressures of the source and ionization chambers were maintained at $\sim 10^{-5}$ and $\sim 10^{-7}$ Torr, respectively, when the nozzle was on. The 355-nm output of a Nd:YAG laser (Spectra-Physics, GCR-150, 10 Hz) was used to pump a dye laser (Lambda-Physik, Scanmate II) to generate laser pulses in the 440–480 nm range. The time duration of the laser pulse was ~6 ns, and the pulse energy was 10–20 mJ/pulse. The laser output was frequency doubled in a BBO crystal placed on a home made autotracking system to maintain both intensity and direction of the doubled laser output while its wavelength was scanned. Tunable UV laser

pulses with a 0.25 cm^{-1} spectral bandwidth were generated in the 220–240 nm region. The UV laser pulse was spatially and temporally overlapped with the molecular beam.

Molecular ions generated via the (1+1) R2PI process were repelled, accelerated, drifted along the field-free region, and detected by microchannel plates (MCP, Jordan) to give the R2PI signal. The ion signal was digitized by an oscilloscope (LeCroy 9361) and stored in a PC, which was also used to control the dye laser and autotracker. The ion signal was monitored as a function of excitation wavelength to give the excitation spectra of methylamines. Absolute wavelengths of the laser output were calibrated using the optogalvanic effect from a hollow-cathode lamp (Ne) within ± 0.5 cm^{-1}.

III. RESULTS AND DISCUSSION

The electronic transition from the ground electronic state to the lowest excited state of methylamine occurs by the excitation of a nitrogen lone-pair electron to a 3*s* Rydberg orbital. The excited state, however, is predissociative even at the origin, indicating that the Rydberg state is strongly coupled to repulsive valence states leading to decomposition of the molecule via N–H, C–N, or C–H bond fission.[8] Therefore, the transition of methylamine to the first-excited state is a bound-to-metastable transition, which carries not only spectroscopic information of the Franck–Condon region, but also dynamic information involved in quantum-specific predissociation processes. In this sense, the R2PI spectra of CH_3NH_2 and CH_3ND_2 provide detailed information about the structure and dynamics of those molecules in the excited states. Since lifetime broadening is much less severe in $CH_3ND_2(\tilde{A})$, peaks representing rotational structures are nicely resolved in the CH_3ND_2 excitation spectrum. Therefore, spectral analyses for CH_3ND_2 are presented here prior to those for CH_3NH_2. The D-to-H substitution effect is then applied for analyzing the CH_3NH_2 excitation spectrum. This section is presented in the following order: (A) internal rotation with symmetry consideration, (B) CH_3ND_2, (C) CH_3NH_2, and (D) tunneling and predissociation.

A. Internal rotation and selection rules

Methylamine is a nonrigid molecule, and thus complete nuclear permutation inversion (CNPI) group theory should be applied for the classification of symmetry species of quantum states.[32] Methylamines in ground and excited states, if tunneling is considered, belong to the G_{12} group. In the ground state, due to tunneling through a sixfold potential for internal rotation, the zero-point energy level is split into six states. Since the torsional barrier in the ground state is relatively high ($V \sim 690\ cm^{-1}$),[19] all six states in the ground vibrational level are split within the energy much less than 0.5 cm^{-1}. Accordingly, in the molecular beam, all of these states are expected to be populated. Vibrational symmetry species of these split states are A_1', A_2'', E', and E'', where E' and E'' states are doubly degenerated. The symmetry species of the total wave functions of CH_3NH_2 and CH_3ND_2 are A_1'' and A_1', respectively, since hydrogen nuclei are fermions while deuterium nuclei are bosons. Therefore, in the ground electronic state of CH_3NH_2 (CH_3ND_2) where $\Gamma^{el}=A_1'$, rovibrational states with even K_a ($\Gamma^{rot}=A_1',A_2'$) and vibrational states of A_1' and E' combine with *para* (*ortho*) states. Meanwhile, rovibrational states with A_1' and E' vibrational symmetry species of CH_3NH_2 (CH_3ND_2) with odd K_a ($\Gamma^{rot}=A_1'',A_2''$) are to be combined with *ortho* (*para*) states. Similarly, rovibrational states with A_2'' and E'' vibrational symmetry species of CH_3NH_2 (CH_3ND_2) with even K_a ($\Gamma^{rot}=A_1',A_2'$) or odd K_a ($\Gamma^{rot}=A_1'',A_2''$) give *ortho* (*para*) or *para* (*ortho*) states, respectively. Nuclear spin statistical weights for *ortho:para* states are 3:1 and 2:1 for CH_3NH_2 and CH_3ND_2, respectively.

The $3s-n$ transition of methylamine is the allowed electric–dipole transition. Analyses of rotational structures of the CH_3ND_2 excitation spectrum indicate for sure that the rotational transition is *b* or *c* type (*vide infra*), indicating that the transition dipole moment is perpendicular to the C–N axis. Since methylamine is the nonrigid molecule and especially since internal rotation is almost free in the excited state, the symmetry of electronic state alone may not be the only criterion for the optical selection rule. In that case, selection rules are determined by considering the symmetry of the direct product of electronic (Γ^{ele}) and internal-rotor (Γ^{int}) symmetry species. Considering nuclear spin conservation in the electronic transition ($\Delta I=0$), ground states of which $\Gamma^{ele''}\otimes\Gamma^{int''}=A_1'$, A_2'', E', and E'' are symmetry allowed to excited states with $\Gamma^{ele'}\otimes\Gamma^{int'}=A_2''$, A_1', E'', and E' (A_1'', A_2', E'', and E'), respectively, for the *c*-type (or *b*-type) transition. However, in the Franck–Condon transition, within the Born–Oppenheimer approximation, the electronic symmetry of the 3*s* Rydberg state is most likely to be A_2'', which correlates to A' or A'' for planar or ciscoid conformers in the C_s (MS) group, respectively. In this case, symmetry species of the internal-rotor states are important criteria for determining selection rules. In other words, for example, in the *c*-type transition, electronically excited internal-rotor states of A_1', A_2'', E', and E'' symmetry species are only symmetry allowed.

A Hamiltonian for the internal and overall rotation including a torsional barrier for methylamines in the excited state can be written as

$$H=H_{rot}+F(p-P)^2+V(\phi), \tag{1}$$

$$V(\phi)=(V_6/2)[1-\cos(6\phi)]. \tag{2}$$

Here H_{rot} is the standard rigid-rotor symmetric-top approximated rotational Hamiltonian and F is the effective rotational constant for the internal rotation of the top about the C–N axis. Since the difference of rotational constants B and C is less than 0.05 cm^{-1},[21] the symmetric-top approximation is good enough within the experimental resolution of this work. The V_6 is the barrier height of a sixfold torsional potential energy surface along the torsional angle ϕ. The $(p-P)$ term represents the relative angular momentum of the top and frame. The free-rotor basis set $\{|m\rangle=(2\pi)^{-1/2}\exp(-im\phi)\}$ is used to construct the Hamiltonian matrix. Nonvanishing matrix elements are as follows:

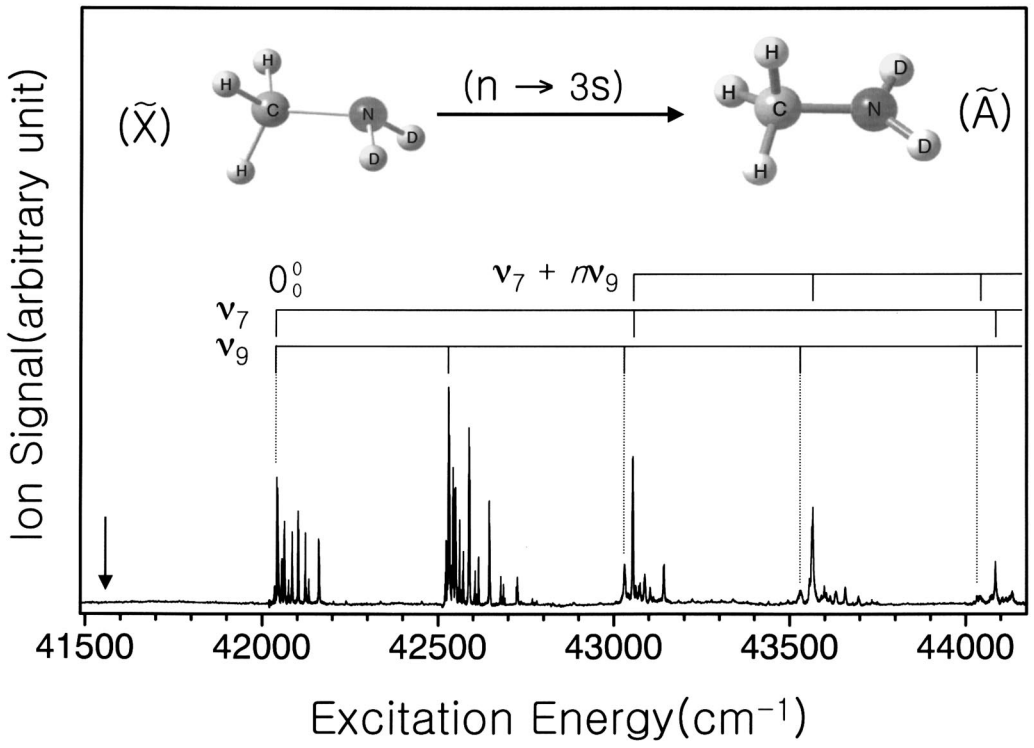

FIG. 1. R2PI excitation spectrum of CH_3ND_2 in the 41 500–44 200 cm^{-1} range. Vibrational bands due to ν_7 (CH_3 rock), ν_9 (ND_2 wag), and their combination modes are appropriately assigned. The peak position expected for the next lower ND_2-wagging band to the spectral origin is indicated as an arrow, which confirms the origin assignment.

$$\langle m|H|m\rangle = (A^{\mathrm{T}}+A^{\mathrm{F}})m^2 + BJ(J+1) + (A^{\mathrm{F}}-B)K'^2 - 2A^{\mathrm{F}}mK' + (V_6/2), \tag{3}$$

$$\langle m|H|m\pm 6\rangle = -(V_6/4). \tag{4}$$

Here A^{T} and A^{F} are rotational constants associated with moments of inertia for the top (I^{top}) and frame (I^{frame}), respectively. In principle, when the internal rotational axis is along the C–N bond, $I=I^{\mathrm{top}}+I^{\mathrm{frame}}$ or, equivalently, $(1/A) = (1/A^{\mathrm{T}}) + (1/A^{\mathrm{F}})$. A 40×40 matrix is diagonalized to give eigenvalues and associated eigenvectors. Symmetry species of internal-rotor wave functions can be classified from eigenvectors deduced from the matrix diagonalization. For example, in the simplest case of $K'=0$ where there is no coupling between overall and internal rotations, the symmetry species of the internal-rotor wave functions which are proportional to $|0\rangle$, $|\pm 1\rangle$, $|\pm 2\rangle$, $[|+3\rangle+|-3\rangle]$, $[|+3\rangle-|-3\rangle]$, $|\pm 4\rangle$, and $|\pm 5\rangle$ are A_1', E'', E', A_2'', A_1'', E', and E'', respectively.[32] It should be noted that, because of the off-diagonal matrix element in Eq. (4), free-rotor basis functions of $m=+3$ and $m=-3$ couple together to generate $(1/2)^{1/2}[|+3\rangle+|-3\rangle]$ or $(1/2)^{1/2}[|+3\rangle-|-3\rangle]$ states of which the symmetry species are A_2'' or A_1'', respectively. As mentioned earlier, the symmetry selection rule indicates that only A_2'', A_1', E'', and E' (A_1'', A_2', E'', and E') states are symmetry allowed in the *c*-type (*b*-type) transition. Thus the upper state of A_1'' or A_2'' is symmetry forbidden for the *c*-type or *b*-type transition, respectively.

B. CH_3ND_2

The CH_3ND_2 excitation spectrum in the 41 500–44 200 cm^{-1} region is shown in Fig. 1 with appropriate vibrational assignments. In Fig. 1, ν_7 and ν_9 represent CH_3 rocking and amino-wagging modes, respectively. Combination bands of ν_7 and ν_9 modes are also clearly identified. Even tiny little bands are not observed at energies below the assigned spectral origin, giving confirmative evidence for the validity of

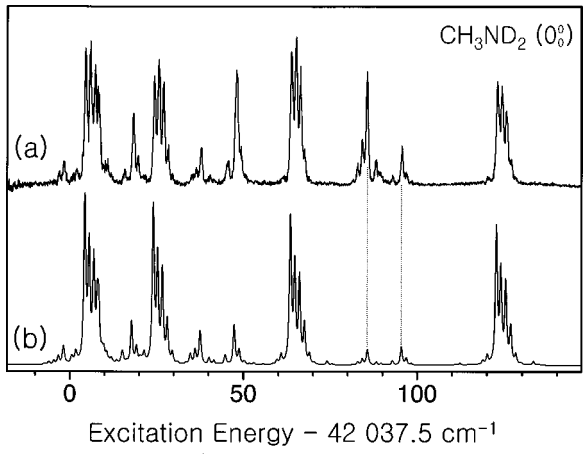

FIG. 2. (a) Excitation spectrum of CH_3ND_2 for the origin band and (b) simulation using parameters listed in Table II. Peaks connected by dotted lines are those very sensitive to the torsional barrier height (see the text for detail).

the origin assignment. The first two bands at the origin and v (ND_2-wag)$=1$ level consist of many sharply resolved peaks, while the bands above $\sim 43\,000$ cm^{-1} show broad spectral features. This indicates that the excited-state lifetime starts to decrease extremely sharply at the v (ND_2-wag)$=2$ level. This is also consistent with the intensity of the R2PI signal, which starts to decrease quite rapidly at the same energy level, Fig. 1. That is, even though the $\tilde{A}-X$ absorption cross section increases as the excitation energy increases in the $42\,000-44\,000$ cm^{-1} range,[26,30] the ionization cross section from intermediate $\tilde{A}$ states decreases in the same energy region. This indicates that the ionization process which occurs competitively with predissociation in the $\tilde{A}$ state becomes much less efficient at vibrational levels where predissociation becomes quite rapid, resulting in a decrease of the R2PI signal. It is interesting to note that the intensity decreasing rate is much faster for ND_2 wagging progression bands compared to that for the CH_3 rocking or its combination bands, Fig. 1.

The origin band of the CH_3ND_2 excitation spectrum consists of relatively sharp peaks, Fig. 2(a). The simulation based on the overall and internal rotor Hamiltonian with a torsional barrier (Sec. III A) is carried out for comparison with experiment. The free-rotor energy expression used in the simulation in our previous report was not perfectly successful in matching all peak positions.[31] However, by introducing a torsional barrier height of 5.0 ± 0.5 cm^{-1}, all experimental peak positions are now perfectly reproduced in the simulation as shown in Fig. 2(b). The internal rotational constants of the top (A^{T}) and frame (A^{F}) are both determined to be 4.93 cm^{-1}. At the zero-point energy level of the excited state, the moments of inertia of the CH_3 and ND_2 group are then found to be identical giving $I'(CH_3)=I'(ND_2)=3.42$ amu Å^2. It is quite interesting that the moments of inertia determined in the experiment are identical for the top (ND_2) and frame (CH_3). Coupling between internal rotations of the top and frame may exist especially when the associated moments of inertia are so similar to each other. A theoretical formulation for describing this interesting behavior is needed in the future. The overall rotational constant B' of the excited CH_3ND_2 in the symmetric-top approximation is found to be 0.67 cm^{-1}. For the ground state of CH_3ND_2, rotational energies are calculated using an asymmetric rotor program.[33] Observed and calculated frequencies associated with transitions between angular momentum quantum numbers of the lower (J'',K_a'',K_c'') and upper (J',K',m') states are listed in Table I. Energy differences between experimental and simulated values are all less than 0.5 cm^{-1}. It should be noted here that a series of peaks due to the excited internal-rotor state with a A_1'' symmetry and wave function of $(1/2)^{1/2}[|+3\rangle-|-3\rangle]$ is absent in the experiment. Accordingly, the corresponding level is excluded in the simulation. This strongly indicates that the $\tilde{A}-X$ transition belong to the *c*-type transition, since in the *c*-type transition the A_1'' upper state is not symmetry allowed (*vide supra*). Rotational selection rules of $\Delta K\,(K'-K_a)=\pm1$, $\Delta J=0$ or ±1 used in the simulation are also consistent with the above. Relative band intensities associated with different upper m' values are arbitrarily scaled in the simulation, while the population of the ground-state methylamine over (J'',K_a'',K_c'') quantum numbers is calculated from the Boltzmann distribution.

Crucial information about the structure and dynamics of excited methylamine is also obtained from other parameters used in the simulation. Parameters used in simulations are listed in Table II with their uncertainties. The rotational temperature of the molecular beam is found to be 3.6 K, indicating that cooling of the sample is quite sufficient. Actually, it is found that Ne is the most effective carrier gas in cooling methylamines in a supersonic jet compared to Ar or He. The exact position for the 0–0 transition is precisely determined to be $42\,038\pm1$ cm^{-1} in the simulation. It is also noteworthy that the zero-point energy due to the torsional mode is 2.49 cm^{-1}, in Table II. This small zero-point torsional energy is important because it varies upon coupling with other vibrational modes (*vide infra*). Predissociation dynamics are also revealed in the spectral bandwidths. The linewidth of individual peaks is much broader than the laser linewidth of 0.25 cm^{-1}. Thus a Gaussian function with a full width at half maximum (FWHM) of 0.25 cm^{-1} is convoluted with a Lorentzian function with an adjustable FWHM, ΔE, to simulate detailed spectral features. The most successful simulation is obtained when $\Delta E\sim0.6$ cm^{-1}, indicating that the corresponding excited state lifetime (τ) is, from $\Delta E\,\tau\sim\hbar$, about 8.8 ps.

The band structure of the first ND_2 wagging mode is very similar to that of the origin band, Fig. 3(a). The simulation matches the experiment perfectly in Fig. 3(b). However, the parameters used in the simulation are different from those used for the origin band, Table II. First of all, the torsional barrier height is found to be increased to 19.0 ± 0.5 cm^{-1} when internal rotation is combined with one quantum in the ND_2 wagging mode. This is an interesting vibrational dependence of the torsional barrier height, as shown in Fig. 4, providing essential information about the coupling of the ND_2 wag and internal rotation. It would be intriguing to compare torsional dynamics of $CH_3ND_2(\tilde{A})$ with those of the $CH_3CH_2(X)$ radical, since the former with one of nonbonding electrons excited to the Rydberg state is expected to have a rather similar electronic structure to that of the latter in the ground electronic state. Moreover, the methylamine cation is isoelectroic to the ethyl radical.[34] Torsional barrier heights of the ethyl radical in the ground electronic state had been determined to be 17 and 10 cm^{-1} for the zero-point and CH_2 wag levels, respectively,[35,36] giving good agreement in general magnitude with values of barrier heights determined for $CH_3ND_2(\tilde{A})$ here. However, the vibrational dependence of the torsional barrier height in the ethyl radical seems to be in the opposite trend compared to that found in $CH_3ND_2(\tilde{A})$.[35,36] This difference of methylamine($\tilde{A}$) and the ethyl(X) radical in the vibrational dependence of the torsional barrier height is interesting and subjected to further investigation.

The zero-point torsional energy is 9.37 cm^{-1}. Thus the 1–0 fundamental transition frequency of 487.0 cm^{-1} for ND_2 wag should be slightly modified to 480.1 cm^{-1} when the difference between zero-point torsional energies of the ground vibrational level and first wagging band is extracted: i.e., $487.0+(2.49-9.37)=480.1$. However, couplings among

TABLE I. Observed and calculated frequencies with angular momentum quantum numbers of ground and excited states for the origin bands in the 42 000–42 200 cm^{-1} region of the CH_3ND_2 excitation spectrum.

Obs. freq.[a] (cm^{-1})	Calc. freq.[b] (cm^{-1})	Excited states[c]			Ground states			Obs.-calc. (cm^{-1})
		J'	K'	m'	J''	K''_a	K''_c	
−3.3	−3.3	0	0	0	1	1	0	0.0
−1.9	−1.9	1	0	0	1	1	1	0.0
	−1.8	2	0	0	2	1	2	−0.1
4.3	4.3	1	1	1	1	0	1	0.0
	4.3	1	1	0	1	0	1	0.0
	4.4	2	1	1	2	0	2	−0.1
	4.4	2	1	0	2	0	2	−0.1
5.7	5.6	1	1	1	0	0	0	0.1
	5.6	1	1	0	0	0	0	0.1
7.1	7.0	2	1	1	1	0	1	0.1
	7.0	2	1	0	1	0	1	0.1
8.0	7.9	2	2	1	1	1	0	0.1
	8.0	1	0	1	1	1	1	0.0
	8.0	1	0	−1	1	1	1	0.0
	8.0	2	2	1	1	1	1	0.0
	8.1	2	0	−1	2	1	2	−0.1
	8.1	2	0	1	2	1	2	−0.1
	8.4	3	1	1	2	0	2	−0.4
	8.4	3	1	0	2	0	2	−0.4
18.0	17.8	2	2	0	1	1	0	0.2
	17.8	2	2	2	1	1	0	0.2
	17.8	2	2	2	1	1	1	0.2
	17.8	2	2	0	1	1	1	0.2
19.3	19.2	3	2	0	2	1	1	0.1
	19.2	3	2	2	2	1	1	0.1
	19.3	3	2	2	2	1	2	0.0
	19.3	3	2	0	2	1	2	0.0
24.1	24.0	1	1	2	1	0	1	0.1
	24.0	1	1	−1	1	0	1	0.1
	24.1	2	1	2	2	0	2	0.0
	24.1	2	1	−1	2	0	2	0.0
	24.2	3	1	2	3	0	3	−0.1
	24.2	3	1	−1	3	0	3	−0.1
25.5	25.3	1	1	2	0	0	0	0.2
	25.3	1	1	−1	0	0	0	0.2
26.7	26.7	2	1	2	1	0	1	0.0
	26.7	2	1	−1	1	0	1	0.0
28.1	28.1	3	1	2	2	0	2	0.0
	28.1	3	1	−1	2	0	2	0.0
36.3	36.1	0	0	2	1	1	0	0.2
	36.1	0	0	−2	1	1	0	0.2
37.7	37.5	1	0	−2	1	1	1	0.2
37.7	37.5	1	0	2	1	1	1	0.2
	37.7	2	0	2	2	1	2	0.0
	37.7	2	0	−2	2	1	2	0.0
47.8	47.3	2	2	−1	1	1	0	0.5
	47.3	2	2	3	1	1	0	0.5
	47.4	2	2	3	1	1	1	0.4
	47.4	2	2	−1	1	1	1	0.4
63.6	63.4	1	1	3	1	0	1	0.2
	63.4	1	1	−2	1	0	1	0.2
	63.5	2	1	3	2	0	2	0.1
	63.5	2	1	−2	2	0	2	0.1
64.9	64.7	1	1	3	0	0	0	0.2
	64.7	1	1	−2	0	0	0	0.2
66.1	66.1	2	1	3	1	0	1	0.0
	66.1	2	1	−2	1	0	1	0.0
67.3	67.5	3	1	3	2	0	2	−0.2
	67.5	3	1	−2	2	0	2	−0.2
82.6	82.9	1	0	[−3, 3]	2	1	1	−0.3
83.9	84.2	0	0	[−3, 3]	1	1	0	−0.3
85.3	85.6	1	0	[−3, 3]	1	1	1	−0.3

TABLE I. (*Continued.*)

Obs. freq.[a] (cm^{-1})	Calc. freq.[b] (cm^{-1})	Excited states[c] J'	K'	m'	Ground states J''	K''_a	K''_c	Obs.-calc. (cm^{-1})
	85.7	2	0	[−3 3	2	1	2	−0.4
95.4	95.4	2	2	[−2 4	1	1	0	0.0
	95.5	2	2	[−2 4	1	1	1	−0.1
96.6	96.8	3	2	[−2 4	2	1	1	−0.2
	96.9	3	2	[−2 4	2	1	2	−0.3
122.8	122.6	1	1	4	1	0	1	0.2
	122.6	1	1	−3	1	0	1	0.2
	122.7	2	1	4	2	0	2	0.1
	122.7	2	1	−3	2	0	2	0.1
124.0	124.0	1	1	4	0	0	0	0.0
	124.0	1	1	−3	0	0	0	0.0
125.3	125.3	2	1	4	1	0	1	0.0
	125.3	2	1	−3	1	0	1	0.0

[a]42 037.5 cm^{-1} is added for absolute transition frequencies.
[b]See Table II for parameters used for the simulation.
[c]Only absolute values of K' are shown here. The internal-rotational quantum number m' is determined from eigenvectors calculated from the Hamiltonian matrix diagonalization using the free-rotor basis set. Since the barrier height is very low ($V_6=5$ cm^{-1}), m' is a nearly good quantum number for excited states with no coupling.

many other vibrational modes are not quantitatively known, and in the more strict sense, such coupling effects are to be all considered in determining fundamental frequency of pure ND_2 wag. Accordingly, in order to be fair, the fundamental frequency of ND_2 wag is reported here to be 487 cm^{-1}. Both A^T and A^F are found to be decreased to 4.86 cm^{-1} in the first ND_2 wagging band, indicating that $I'(CH_3)=I'(ND_2)=3.47$ amu Å^2. This indicates that angles and bond lengths become more relaxed at the first wagging vibrational level compared to those at the origin. Applying a simple formula $A^T(v)=A_e^T-\alpha_e(v+\frac{1}{2})$ or $A^F(v)=A_e^F-\alpha_e(v+\frac{1}{2})$, it is found that $A_e^T=A_e^F=4.97$ cm^{-1} while $\alpha_e=0.07$ cm^{-1}. Corresponding values calculated from the *ab initio* geometry (CASSCF with a 6-31++G**) of the excited CH_3ND_2 calculated by the Morokuma group[8] are $I'(CH_3)=3.16$ and $I'(ND_2)=3.01$ amu Å^2. Moments of inertia for both of the ND_2 and CH_3 groups shows relatively poor agreement with the experiment. This means that, for instance, the D–N–D angle is actually larger than the *ab initio* value of 116.5°.[8] Namely, if the *ab initio* value of 1.020 Å is taken for the N–D bond length in the excited state,[8] then the experimental value of A_e^T predicts a D–N–D angle of 129°, suggesting that better understanding of the excited-state geometry of methylamine would benefit from more advanced theoretical calculations. The overall rotational constant B' is also slightly decreased to 0.66 cm^{-1}. The individual linewidth is identical to that in the origin band, indicating that the excited-state lifetime of the first wagging band remains at ~8.8 ps.

The most dramatic change in vibrational bands due to $2\nu_9$ and ν_7 is the much more broadened linewidths compared to those in the origin and ν_9 bands, Fig. 5(a). Accordingly, in the simulation for the $2\nu_9$ band in Fig. 5(b), it is found that $\Delta E\sim3.0$ cm^{-1}, corresponding to $\tau\sim1.8$ ps. Because of broadened linewidths, spectral features due to over-

TABLE II. Parameters used in the simulation for CH_3ND_2 excitation spectra.[a]

	0_0^0	ν_9	$2\nu_9$	ν_7	$3\nu_9$	$\nu_7+\nu_9$	$4\nu_9$	$\nu_7+2\nu_9$	$2\nu_7$
A^T	4.93±0.05	4.86±0.05	(4.77)	(4.5)	(4.1)	(3.9)	(4.6)	(4.6)	(4.1)
A^F	4.93±0.05	4.86±0.05	(4.77)	(4.5)	(4.1)	(3.9)	(4.6)	(4.6)	(4.1)
A	2.465±0.05	2.43±0.05							
B'	0.67±0.01	0.66±0.01	(0.65)	(0.65)	(0.64)	(0.68)	(0.58)	(0.58)	(0.50)
FWHM	0.60±0.05	0.60±0.05	3.0±0.5	1.3±0.5	8±1	2.0±1.0	(8.0)	(8.0)	>8.0
τ (ps)	8.8±0.7	8.8±0.7	1.8±0.3	4.1±0.5	0.7±0.1	2.6±0.8	(0.7)	(0.7)	<0.7
V_6	5.0±0.5	19.0±0.5	22±1	(9.0)	(25)	(25)			(25)
ZPE (torr)[b]	2.49±0.25	9.37±0.25	10.8±0.5	(4.47)	(12.24)	(12.22)			(12.24)
E_{vib}	0 [42038±1]	487±1	988±1	1012±1	1490±2	1522±2	1989±2	1997±2	2042±2

[a]Parameters in parentheses are less reliable.
[b]Zero-point energy due to torsional motion.

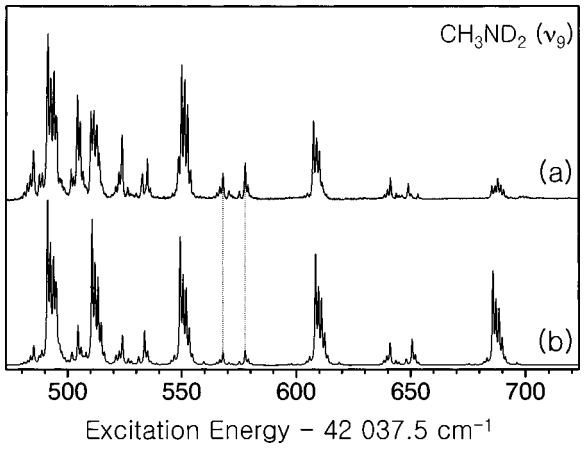

FIG. 3. (a) Excitation spectrum of CH_3ND_2 for the ν_9 (ND_2 wag) band and (b) simulation using parameters listed in Table II. Peaks connected by dotted lines are those very sensitive to the torsional barrier height, which is 19 cm^{-1} in this band.

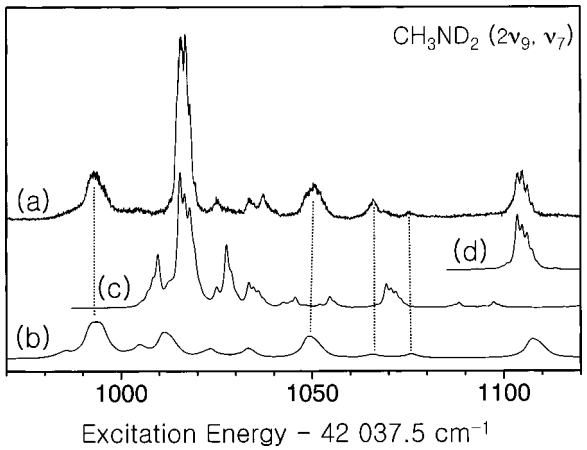

FIG. 5. (a) Excitation spectrum of CH_3ND_2 for the $2\nu_9$ and ν_7 bands and the simulation for (b) $2\nu_9$ and (c) ν_7 bands using parameters listed in Table II. The simulation for a series of peaks at $\sim$1110 cm^{-1} is shown in (d). It should be noted that linewidths are quite different for different modes.

all rotation are not resolved, and $B=0.65\,cm^{-1}$ is simply assumed in the simulation. The vibrational energy of $2\nu_9$ is determined to be 988 cm^{-1}, Table II. If the anharmonicity constant due to the ν_9 mode, χ_{99}, is only considered to be significant, then using a simple anharmonic formula $E_{\mathrm{vib}}(v)=\omega_e(v+\frac{1}{2})+\chi_{99}(v+\frac{1}{2})^2$ together with fundamental and first overtone frequencies of 487 and 987.5 cm^{-1}, respectively, it is found out that $\omega_e=473\,cm^{-1}$ and $\chi_{99}=7.0\,cm^{-1}$. The positive value of χ_{99} in the excited planar CH_3ND_2 is as expected since two ground-state potentials separated by a wagging barrier become merged in the excited state, which is similarly observed in the inversion mode of the NH_3 excited state.[9] The best fitting value of $A^{\mathrm{T}}(2)$ or $A^{\mathrm{F}}(2)$ is found to be 4.77 cm^{-1} in the $2\nu_9$ band, and this value is very close to 4.79 cm^{-1}, which is calculated from A_e^{T}, A_e^{F}, and α_e values deduced from accurately and precisely determined internal rotational constants $A^{\mathrm{T}}(0)$, $A^{\mathrm{F}}(0)$, $A^{\mathrm{T}}(1)$, and $A^{\mathrm{F}}(1)$ (*vide supra*). The torsional barrier height in the $2\nu_9$ band is determined to be 22 ± 1 cm^{-1} in the simulation, although it should be noted that this value is not completely conclusive since associated rotational structures are not clearly resolved in the $2\nu_9$ band. Meanwhile, the strong peak at the vibrational energy of 1012 cm^{-1} ascribed to ν_7 (CH_3 rocking) requires a linewidth of $\sim$1.3 cm^{-1} for the simulation in Fig. 5(c), giving an associated lifetime of $\sim$4.1 ps. The longer lifetime of the ν_7 band compared to that of $2\nu_9$ is also consistent with the higher intensity of the former compared to that of the latter. This is an interesting mode dependence of the predissociation rate, which will be discussed more in Sec. III D. It is also interesting to note that a series of peaks at the rovibrational energy of $\sim$1110 cm^{-1} above the origin is partly rotationally resolved, Fig. 5(a). Assignments of these peaks are not certain at the present time. However, in order to reproduce these partly resolved rotational structures, a linewidth of $\Delta E\sim1.2\,cm^{-1}$ has to be used in the simulation, Fig. 5(d). The corresponding lifetime is $\sim$4.4 ps, and this is much longer than the $2\nu_9$ lifetime, while it is very similar to the ν_7 lifetime. Actually, in the following paper,[34] these peaks are found to have ν_7 mode character.

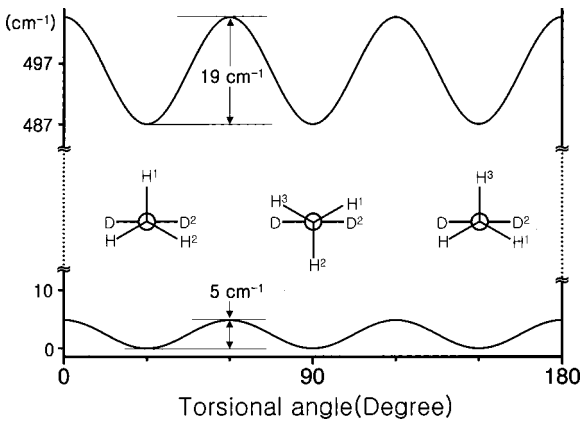

FIG. 4. Model potential $V(\phi)=(V_6/2)[1-\cos(6\phi)]$, for the internal rotation of ND_2 with respect to CH_3 along the C–N axis. The V_6 of 5 cm^{-1} at the origin becomes 19 cm^{-1} at the ν_9 band. The planar geometry of CH_3ND_2 in the excited state is assumed to be more stable according to the *ab initio* calculation in Ref. 8.

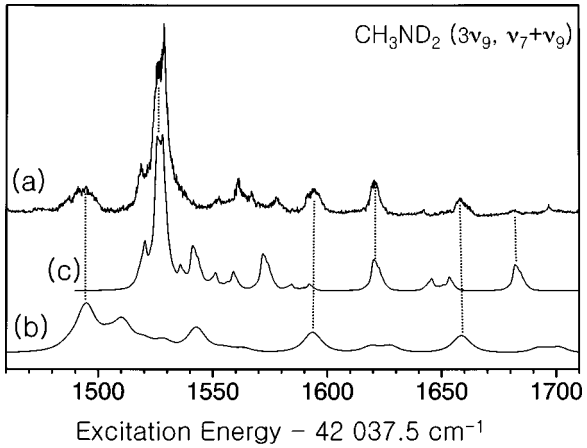

FIG. 6. (a) Excitation spectrum of CH_3ND_2 for the $3\nu_9$ and $\nu_7+\nu_9$ bands and the simulation for (b) $3\nu_9$ and (c) $\nu_7+\nu_9$ bands using parameters listed in Table II.

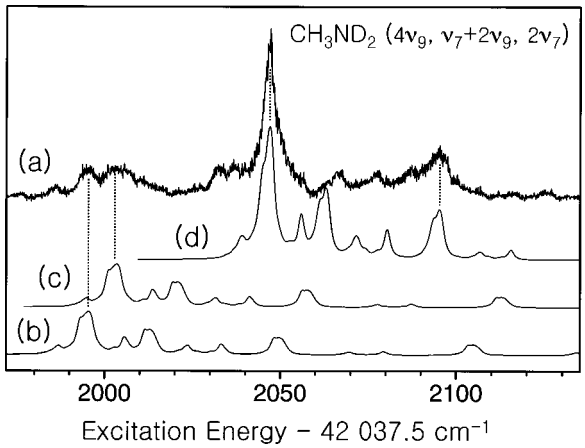

FIG. 7. (a) Excitation spectrum of CH_3ND_2 for the $4\nu_9$, $\nu_7+2\nu_9$, and $2\nu_7$ bands and the simulation for (b) $4\nu_9$, (c) $\nu_7+2\nu_9$, and (d) $2\nu_7$ bands using parameters listed in Table II.

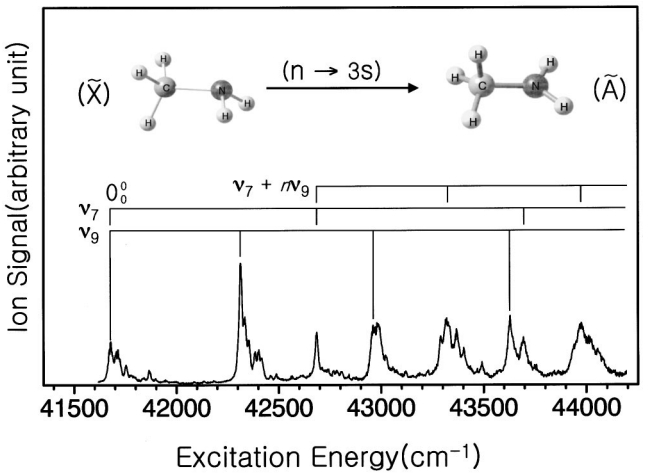

FIG. 9. R2PI excitation spectrum of CH_3NH_2 in the 41 500–44 000 cm^{-1} range. Vibrational bands due to ν_7 (CH_3 rock), ν_9 (NH_2 wag), and their combination modes are appropriately assigned.

Vibrational bands due to $3\nu_9$ and $\nu_7+\nu_9$ bands are shown in Fig. 6(a). Simulations for $3\nu_9$ and $\nu_7+\nu_9$ bands based on the parameters listed in Table II show good agreement with the experiment in Figs. 6(b) and 6(c), respectively. The vibrational term value of $3\nu_9$ is determined to be 1490 cm^{-1}. Calculation of vibrational energy using value of $\omega_e = 473\,cm^{-1}$ and $\chi_{99}=7.0\,cm^{-1}$, deduced from precisely determined term values of ν_9 and $2\nu_9$, gives a $3\nu_9$ vibrational energy of 1503 cm^{-1} (*vide supra*), which is very close to the above experimental value of 1490 cm^{-1}. The linewidth in the simulation for $3\nu_9$ is ~8.0 cm^{-1}, corresponding to τ~0.7 ps, indicating that the lifetime gets even shorter when the vibrational energy is given as three quanta of ND_2 wag. Meanwhile, a linewidth of ~2 cm^{-1} (τ~2.6 ps) seems to match the experiment pretty well for the $\nu_7+\nu_9$ band, indicating once again that the lifetime gets longer when a part or whole of the vibrational energy is deposited onto the CH_3 rocking mode. The vibrational term value for $\nu_7+\nu_9$ is determined to be 1522 cm^{-1}. A direct sum of the fundamental frequencies of ν_7 and ν_9 is 1499 cm^{-1}, and thus the anharmonic coupling of ν_7 and ν_9 seems to be significant. However, the torsional barrier height cannot be deduced accurately, while it is true that it varies with different combinations of vibrational modes. Accordingly, a quantitative description of the anharmonic coupling between ν_7 and ν_9 modes seems to need more spectroscopic data.

The broad peaks found at an internal energy of ~2000 cm^{-1} are due to $4\nu_9$, $\nu_7+2\nu_9$, and $2\nu_7$ bands, Fig. 7(a). Overall, most of bands are diffuse in nature, indicating ultrashort lifetimes of excited states in this energy region. As shown in Fig. 1, the band intensity at this energy is relatively very low, though the corresponding absorption cross section should be most intense at such internal energies. Molecular constants deduced from simulations for these low-intensity broadbands are thus less reliable. The lower bound for a linewidth of ~8 cm^{-1} is used for the simulation for $4\nu_9$, $\nu_7+2\nu_9$, and $2\nu_7$ bands as shown in Figs. 7(b), 7(c), and 7(d), respectively, with their respective vibrational term values of 1989, 1997, and 2042 cm^{-1}, Table II. These term values for overtones or combinations of ν_7 and ν_9 would be

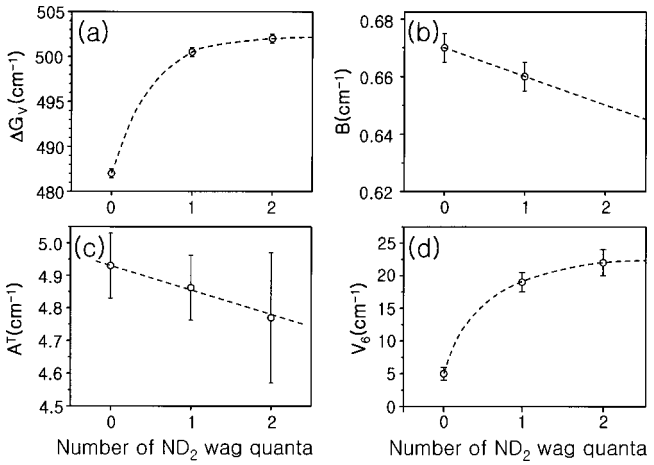

FIG. 8. Dependencies of molecular constants of excited CH_3ND_2 with the number of ND_2 wagging quanta: (a) $\Delta Gv=G(v+1)-G(v)$, (b) B', (c) $A^T(=A^F)$, and (d) V_6. Only reliable data are plotted here (see Table II).

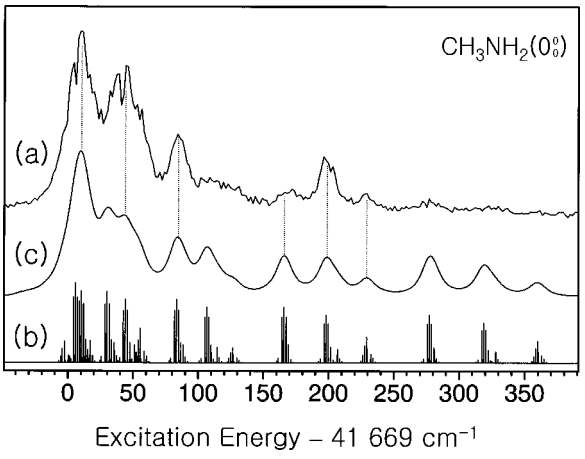

FIG. 10. (a) Excitation spectrum of CH_3NH_2 for the origin band, (b) the simulation with a stick spectrum, and (c) the simulation with an individual linewidth of 14 cm^{-1}. Parameters used in the simulation are listed in Table III.

TABLE III. Parameters used in the simulation for CH_3NH_2 excitation spectra.[a]

	0_0^0	ν_9	ν_7	$2\nu_9$	$\nu_7+\nu_9$	$3\nu_9$	$2\nu_7$	$\nu_7+2\nu_9$
A^T	9.57±0.10	8.54±0.1	(9)	(8)	(10.4)	(7.2)	(7.2)	(10.4)
A^F	4.93±0.10	4.86±0.1	(6)	(4)	(4.8)	(4.8)	(4.8)	(4.8)
B'	(0.78)	(0.77)	(0.77)	(0.76)	(0.77)	(0.74)	(0.74)	(0.77)
FWHM	14±1	13±1	12±1	16±2	12±2	18±3	18±3	>22
τ (ps)	0.38±0.03	0.41±0.03	0.44±0.03	0.33±0.04	0.44±0.08	0.29±0.06	0.29±0.06	<0.24
V_6	(5)	(19)	(20)					
ZPE (torr)[b]	(2.49)	(9.41)	(9.9)					
E_{vib}	0 [41669±1]	636±1	1008±1	1285±2	1549±10	1952±2	2014±5	2266±10

[a]Parameters in parentheses are less reliable.
[b]Zero-point energy due to torsional motion.

quite helpful in the construction of potential energy surfaces of this floppy molecule in its predissociative excited state especially at near the top of the reaction barrier along the specific bond-dissociation coordinate. Only accurately determined values for $\Delta Gv = G(v+1) - G(v)$, B, A^T, and V_6 are plotted with the number of quanta in ND_2 wag in Fig. 8. It is interesting to note that both ΔGv and V_6 show leveling offs as the number of ND_2 wag quanta increases, while B and A^T values are on a straight line. A detailed theoretical calculation of multidimensional potential energy surfaces would be desirable to explain the experiment.

C. CH_3NH_2

The CH_3NH_2 excitation spectrum taken in the 41 500–44 200 cm^{-1} range is shown in Fig. 9 with appropriate vibrational assignments. Similar to the case of CH_3ND_2, ν_7 (CH_3 rock), ν_9 (NH_2 wag), and a combination of ν_7 and ν_9 bands are clearly identified in the CH_3NH_2 excitation spectrum. Spectral bandwidths, however, are much broader than those of CH_3ND_2, indicating much shorter lifetimes of CH_3NH_2 ($\tilde{A}$). The vibrational frequency of the amino-wagging mode is much blueshifted by D-to-H substitution of the amino moiety, while the CH_3 rocking frequency remains more or less the same. The origin band of the CH_3NH_2 excitation spectrum shown in Fig. 10(a) is not rotationally well resolved due to severe homogeneous line broadening. In the first place, the CH_3NH_2 simulation can be tried by applying the effect of the NH_2-to-ND_2 substitution to molecular constants deduced from the CH_3ND_2 simulation. In CH_3NH_2, A^T and A^F are quite distinct. Assuming that the minimum-energy geometries of excited CH_3ND_2 and CH_3NH_2 are identical, the moments of inertia of CH_3 and NH_2 are then determined from those deduced from CH_3ND_2 to give $I'(CH_3) = 3.42$ amu Å^2 and $I'(NH_2) = 1.71$ amu Å^2 (*vide supra*), since the moment of inertia of NH_2 is simply the double of that of ND_2. Then $A^T = 9.86\ cm^{-1}$ and $A^F = 4.93\ cm^{-1}$ are expected. However, for the best fit of the experiment, A^T has to be decreased to 9.57 cm^{-1}. This difference should come from different vibrational mode couplings of CH_3NH_2 and CH_3ND_2 even at their origins (*vide infra*). Accordingly, the internal rotational constants of $A^T = 9.57\ cm^{-1}$ and $A^F = 4.93\ cm^{-1}$ are used in the simulations in Fig. 10. The overall rotational constant B' of the excited CH_3NH_2 in the symmetric-top approximation is assumed to be 0.78 cm^{-1} compared to $B' = 0.67\ cm^{-1}$ for CH_3ND_2, deduced from the comparison of $(B+C)/2 = 0.738$ and 0.648 cm^{-1} of the electronically ground CH_3NH_2 and CH_3ND_2, respectively.[21] The torsional barrier height is presumed to be identical, $V_6 = 5\ cm^{-1}$, to that of the CH_3ND_2 origin band. Parameters used in the simulation with their uncertainties are listed in Table III. The simulation with a stick spectrum represents the peak positions and relative intensities, Fig. 10(b). For fitting the real experimental spectrum, the Lorentzian function with a FWHM of 14 cm^{-1} is convoluted to give the simulation in Fig. 10(c). The simulation matches the experiment extremely well, and this indicates that the lifetime of the excited CH_3NH_2 at the origin is ~0.38 ps. This perfect match between experiment and simulation also validates the Hamiltonian in Eqs. (1)–(4) employed in this work. The 0–0 transition frequency is accurately determined to be 41 669 cm^{-1} from the simulation.

The first NH_2 wagging band is very similar to the origin band in its shape and structure, Fig. 11(a). For the simulation of this band, molecular constants determined for the ND_2 wagging band of CH_3ND_2 are adjusted considering the NH_2-to-ND_2 substitution effect. Accordingly, $A^T = 8.54\ cm^{-1}$ and $A^F = 4.86\ cm^{-1}$ are used in the simulation

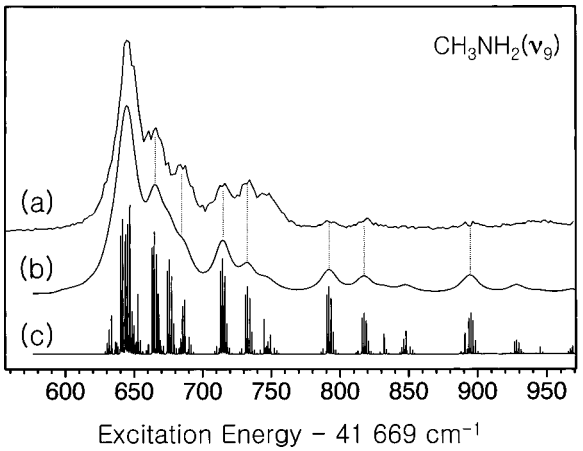

FIG. 11. (a) Excitation spectrum of CH_3NH_2 for the ν_9 (NH_2 wag) band, (b) the simulation with an individual linewidth of 13 cm^{-1}, and (c) the simulation with a stick spectrum. Parameters used in the simulation are listed in Table III.

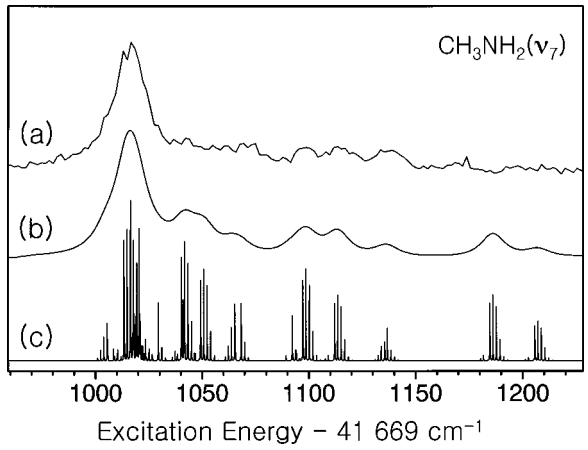

FIG. 12. (a) Excitation spectrum of CH_3NH_2 for the ν_7 band, (b) the simulation with an individual linewidth of 13 cm^{-1}, and (c) the simulation with a stick spectrum. Parameters used in the simulation are listed in Table III.

for the first NH_2 wagging band. From the A^T values determined at the origin and ν_9 bands, A_e^T and α_e^T are calculated to be 10.1 and 1.03 cm^{-1}, respectively. It is very intriguing to note that the A_e^T of CH_3NH_2 (10.1 cm^{-1}) is nearly twice as large as that of CH_3ND_2 (4.97 cm^{-1}). This proves that excited-state structures of CH_3NH_2 and CH_3ND_2 are almost identical at their minimum potential energies. The overall rotational constant B' is assumed to be 0.77 cm^{-1}. A torsional barrier height of 19 cm^{-1} is used, as in the CH_3ND_2 case. A linewidth of 13 cm^{-1} is used for the simulation in Fig. 11(b), and its stick spectrum is shown in Fig. 11(c). The agreement between experiment and simulation is excellent, giving a lifetime of ~0.41 ps for the excited CH_3NH_2 at the first NH_2 wagging band. The fundamental frequency for the NH_2 wag is accurately determined to be 636 cm^{-1}. This is slightly larger than a corresponding value of 603.51 cm^{-1} from *ab initio* calculations.[8]

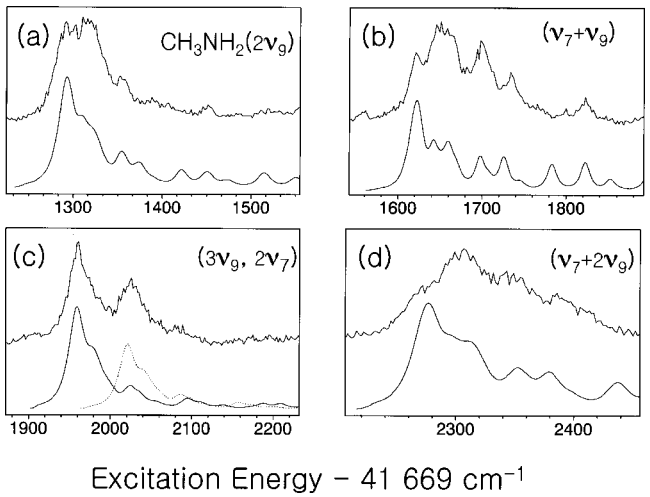

FIG. 13. Excitation spectrum (upper trace) with simulation (lower trace) of excited CH_3NH_2 for (a) $2\nu_9$, (b) $\nu_7+\nu_9$, (c) $3\nu_9/2\nu_7$, and (d) $\nu_7+2\nu_9$ bands using parameters listed in Table II. In (c), the lower left trace is the simulation for the $3\nu_9$ band, while the simulation for $2\nu_7$ is shown as the lower right trace.

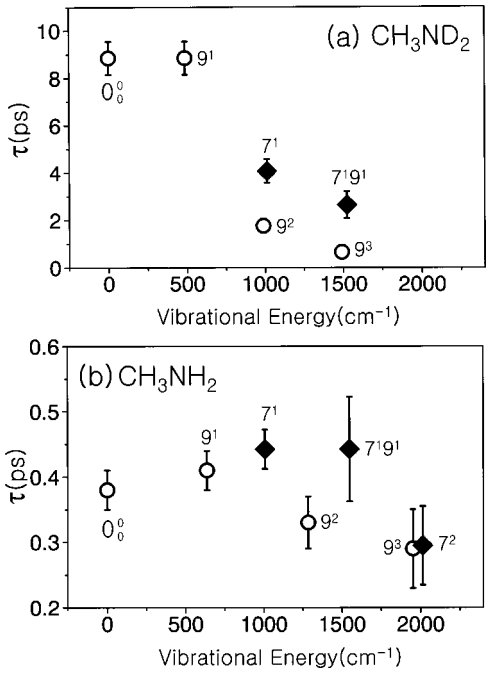

FIG. 14. (a) Lifetimes of excited CH_3ND_2 vs the vibrational energy, which clearly show a strong mode dependence of the lifetime and (b) lifetimes of excited CH_3NH_2 vs the vibrational energy. Note the different time scale on vertical axes in (a) and (b).

The ν_7 band is very well isolated in the CH_3NH_2 excitation spectrum, Fig. 12(a). Highly excited internal rotor states, compared to those of NH_2 wag, are found to be less intense. Accordingly, the molecular constants used in the simulations in Figs. 12(b) and 12(c) are less reliable. However, the fundamental frequency of CH_3 rock is accurately determined in the simulation to give $\nu_7(1-0) = 1008\,\text{cm}^{-1}$. *Ab initio* frequencies for ν_7 and ν_8 are reported to be 1174 and 1051 cm^{-1}, respectively.[8] Thus simple comparison of the experiment with *ab initio* calculation could lead to a different assignment that the 1008 cm^{-1} band is due to ν_8. Previous studies of various isotope analogs of methylamines provided solid evidence for the ν_7 assignment for this band.[26] In addition, a frequency shift by NH_2/ND_2 substitution of ν_8 is expected to be much larger compared to that of ν_7,[8] and thus 1008 cm^{-1} is assigned as the CH_3 rocking mode. This is very close to the value of 1012 cm^{-1} for the ν_7 fundamental frequency of CH_3ND_2. The fact that the ν_7 fundamental frequency of CH_3ND_2 is higher than that of CH_3NH_2 could be due to different anharmonicites among vibrational modes of two isotope species. Further spectroscopic works on CD_3NH_2 and CD_3ND_2 would be quite helpful in unraveling anharmonicities in great detail. The bandwidth of 12 cm^{-1} is used in the ν_7 band simulation in Fig. 12(b) for the best match to the experiment, giving a lifetime of ~0.44 ps, which is slightly longer than that of the origin or first wagging band.

Experimental and simulated spectra for $2\nu_9$, $\nu_7+\nu_9$, $3\nu_9$, $2\nu_7$, and $\nu_7+2\nu_9$ bands are shown in Fig. 13. All peaks are found to be diffuse: thus, molecular constants related to overall and internal rotation are not expected to be deduced accurately from simulations. However, associated

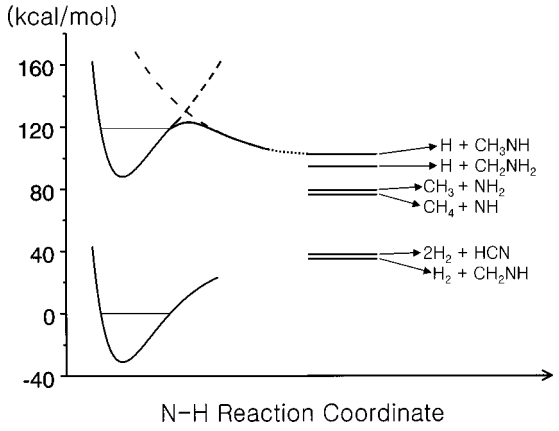

FIG. 15. Simple diagram of potential energy surfaces along the N–H(D) bond dissociation coordinate. Thermodynamically accessible reaction channels are shown on the right (Ref. 4). For the upper state, the adiabatic potential energy surface is depicted in the vicinity of the Franck–Condon region. Thereafter, it correlates to the $H+CH_3NH(X)$ products diabatically in the late stage along the reaction coordinate (Ref. 8).

vibrational energies are relatively quite accurately determined from simulations in Fig. 13, Table III. The vibrational energy of $2\nu_9$ is determined to be 1285 cm^{-1}. Using the equation $E_{vib}(v)=\omega_e(v+1/2)+\chi_{99}(v+\frac{1}{2})^2$ and a ν_9 fundamental frequency of 636 cm^{-1}, it is found out that $\omega_e(NH_2)=623\,cm^{-1}$ and $\chi_{99}(NH_2)=6.5\,cm^{-1}$. The $\chi_{99}(NH_2)$ is very similar to that of ND_2 wag (*vide supra*). These constants predict the vibrational energy of $3\nu_9$ to be 1947 cm^{-1}, which is very close to the experimental value of 1952 cm^{-1}, Table III. Vibrational energy term values for $\nu_7+\nu_9$, $2\nu_7$, and $\nu_7+2\nu_9$ bands are found to be 1549, 2014, and 2266 cm^{-1}, respectively, while harmonic sums using ν_7 and ν_9 fundamentals give respective values of 1644, 2016, and 2293 cm^{-1}. These values for overtones or combinations of ν_7 and ν_9 would be quite helpful in disentangling potential energy surfaces of this floppy molecule in its predissociative excited state. Lifetimes for these bands are also deduced from the simulations and listed in Table III.

D. Tunneling and predissociation

At the origin and ν_9 bands, the excited CH_3ND_2 lifetime ($\sim$8.8 ps) is about 20 times longer than the CH_3NH_2 lifetime ($\sim$0.38 ps) at its origin, Fig. 14. This huge difference in lifetimes of excited CH_3NH_2 and CH_3ND_2 is compelling evidence of tunneling as a predissociation mechanism especially at the origin and first amino-wag bands. Other nonradiative processes such as internal conversion and intersystem crossing do not seem to be responsible for the short lifetimes of excited methylamines, since such electronic dephasing processes are expected to be faster for CH_3ND_2 compared to those for CH_3NH_2 due to the higher densities of low-lying states of the former. Many reaction channels such as N–H, C–H, and C–N bond dissociations are energetically accessible from methylamine in the $\tilde{A}$ state, Fig. 15. However, the huge effect on the predissociation rate by the H/D substitution of amino moiety is not expected in dissociation channels not involving the N–H(D) bond breakage. Therefore, at least at the origin and first wagging vibrational levels, predissociation of CH_3ND_2 occurs via tunneling through a barrier to produce mainly $D+CH_3ND(X)$ fragments. At the $2\nu_9$ energy level of CH_3ND_2, the lifetime becomes much shorter, giving $\tau\sim$1.8 ps. This sudden decrease of the lifetime indicates that predissociation of CH_3ND_2 may occur at near or above the top of the barrier at a vibrational energy of $\sim$1000 cm^{-1}. Actually, the experimental fact that the lifetime is $\sim$0.38 ps at the origin of CH_3NH_2 and it varies little upon increasing the vibrational energy, Fig. 14, strongly suggests that predissociation of CH_3NH_2 may take place at near the top of the barrier even at the zero-point energy level. The difference in zero-point energies of CH_3NH_2 and CH_3ND_2 for the N–H(D) stretching mode, which is the reaction coordinate for the N–H(D) bond cleavage, may account for the difference of reaction barrier heights that CH_3NH_2 and CH_3ND_2 experience along the N–H(D) reaction coordinate. This seems to be consistent with a conclusion by the Ashfold group[5,6] that the dominant predissociation channel of methylamine is the N–H(D) fission process. However, it should be noted that our work confirms only that the major dissociation channel is the N–H(D) bond cleavage at the origin and ν_9 levels of the excited CH_3ND_2 and maybe at the origin level of the excited CH_3NH_2. At higher vibrational energies, however, the tunneling effect fades away as indicated in Fig. 14, and thus other reaction channels are not conclusively excluded from our experimental results.

An interesting mode dependence of the lifetime is quite clearly observed for CH_3ND_2, Fig. 14(a). That is, as clearly shown in Fig. 14(a), lifetimes of ν_7 and its combination bands are about two times longer that those of isoenergetic ν_9 overtone bands. The same trend is also observed in lifetimes of CH_3NH_2, though the mode dependence is less dramatic, Fig. 14(b). A similar mode dependence on the excited lifetime had been reported for N–H bond dissociation of ammonia.[9] For ammonia, thorough experimental and theoretical studies were carried out to reveal fundamental aspects of mode-dependent lifetimes.[9–15] However, for methylamine, our work provides mode-dependent lifetimes for the first time. Both amino-wagging and methyl-rocking modes are perpendicular to the reaction coordinates for bond dissociations. Thus, in the case of no intramolecular vibrational redistribution (IVR), these vibrational modes, which are perpendicular to the reaction coordinate, could survive until the excited molecule reaches the transition state, giving vibrational adiabatic potential energy surfaces characteristic to each vibrational mode. In this case, the mode dependence of the lifetime could be qualitatively explainable. The amino-wag frequency is expected to be lowered at the transition state compared to that of the excited reactant since one of the N–H bonds gets lengthened at the transition state. Meanwhile, the CH_3 rock frequency at the transition state is expected to be more or less same as that of the reactant, since the CH_3 group is not likely to be coupled to the N–H(D) reaction coordinate. Therefore, in this case, the state excited in the CH_3 rocking mode will experience a higher effective reaction barrier. For a better understanding of this interesting mode dependence, multidimensional potential surfaces in the vicinity of the transition state would be needed. More practically, calculation of two-dimensional potential energy sur-

faces including amino wagging or CH_3 rocking would be desirable.

It is also interesting to note that, within the Born–Oppenheimer approximation, the zero-point energy difference between CH_3NH_2 and CH_3ND_2 in the excited state ($\Delta ZPE'$) is calculated to be 1018 cm^{-1} and this is much smaller than that of 1387 cm^{-1} for the ground electronic state ($\Delta ZPE''$). The latter is from experimental values,[21] while the former is calculated from the latter and origin energies of CH_3NH_2 and CH_3ND_2: $\Delta ZPE' = T_{00}(CH_3NH_2) + \Delta ZPE'' - T_{00}(CH_3ND_2) = 41\,669 + 1387 - 42\,038 = 1018$. This huge difference between $\Delta ZPE'$ and $\Delta ZPE''$ is quite rare, since the NH_2/ND_2 substitution would affect the zero-point energies almost equally for the ground and excited states. Therefore, this indicates that potential energy surfaces especially along N–H(D) stretching coordinates are quite anharmonic in the excited state compared to those in the ground state. That is, the more anharmonic excited potential energy surface gives the lower zero-point N–H(D) stretching frequency, resulting in a decrease of the zero-point energy difference between CH_3NH_2 and CH_3ND_2. This anharmonicity should come from severe coupling of the $3s-n$ Rydberg state and repulsive valence state along the N–H(D) dissociation coordinate. Detailed *ab initio* calculations of the coupling region of Rydberg and valence states would be desirable for a quantitative explanation of this interesting experimental observation.

IV. CONCLUSIONS

Here rovibrational structures and dynamics of methylamines (CH_3NH_2 and CH_3ND_2) in predissociative $\tilde{A}$ states ($3s-n$) are revealed through (1+1) resonant-enhanced two-photon ionization spectroscopy. Spectral origins are accurately and precisely determined through the simulation to be 41 669 and 42 038 cm^{-1} for CH_3NH_2 and CH_3ND_2, respectively. The amino group which is bent in the ground electronic state becomes planar in the excited methylamine. Due to this geometrical change upon electronic excitation, amino-wagging and CH_3-rocking modes are found to be optically active, giving their respective fundamental frequencies of 636 (487) and 1008 (1012) cm^{-1} for CH_3NH_2 (CH_3ND_2). In the excited state, CH_3 rotates nearly freely about the C–N axis with respect to $NH_2(ND_2)$. For CH_3ND_2 ($\tilde{A}$), torsional barriers of 5 and 19 cm^{-1} are accurately determined for the zero-point and first amino-wagging levels, respectively, through the simulation using the internal-rotor Hamiltonian with a sixfold potential function. Lifetimes of quantum states in excited methylamines are estimated from spectral linewidths to give ~8.8 and ~0.38 ps for zero-point levels of CH_3ND_2 and CH_3NH_2, respectively. The huge NH_2/ND_2 isotopic substitution effect on the excited-state lifetime strongly indicates that the primary dissociation channel of excited methylamine is the N–H(D) bond dissociation and it proceeds via tunneling through a reaction barrier at least at low vibrational energies. At the vibrational energy of ~1000 cm^{-1}, the lifetime of CH_3ND_2 suddenly drops to 1.8 ps, suggesting a comparable reaction barrier height along the N–D reaction coordinate. Lifetimes of excited methylamines are systematically measured here to give an interesting mode dependence of the lifetime. Lifetimes of states with the CH_3-rocking mode excited are longer than those of isoenergetic ND_2-wagging modes. Multidimensional potential energy surfaces near the reaction barrier along the N–H(D) reaction coordinate would be extremely helpful for a better understanding of these interesting experimental facts in regard to mode-dependent lifetimes. In conclusion, quantum states of CH_3NH_2 and CH_3ND_2 in their first-excited states are clearly characterized in this work. Since the excited molecule predissociates, methylamine serves as an excellent model system for state-to-state reaction dynamics studies. The effect of initial quantum reactant states on the reaction outcome is an always-stimulating subject. Thus more dynamics studies along this direction with theoretical calculations are needed.

ACKNOWLEDGMENTS

This work was financially supported by Korea Research Foundation Grant No. KRF-2002-070-C00046. The discussion with Professor W. H. Miller at UC Berkeley was very brief, but very helpful.

[1] J. V. Michael and W. A. Noyes, J. Am. Chem. Soc. **85**, 1228 (1963).
[2] E. P. Gardner and J. R. McNesby, J. Phys. Chem. **86**, 2646 (1982).
[3] H. K. Haak and F. Stuhl, J. Phys. Chem. **88**, 3627 (1984).
[4] G. C. G. Waschewsky, D. C. Kitchen, P. W. Browning, and L. J. Butler, J. Phys. Chem. **99**, 2635 (1995).
[5] C. L. Reed, M. Kono, and M. N. R. Ashfold, J. Chem. Soc., Faraday Trans. **92**, 4897 (1996).
[6] M. N. R. Ashfold, R. N. Dixon, M. Kono, D. H. Mordaunt, and C. L. Reed, Philos. Trans. R. Soc. London, Ser. A **355**, 1659 (1997).
[7] T.-X. Xiang and W. A. Guillory, J. Chem. Phys. **85**, 2019 (1986).
[8] K. M. Dunn and K. Morokuma, J. Phys. Chem. **100**, 123 (1996).
[9] A. Bach, J. M. Hutchison, R. J. Holiday, and F. F. Crim, J. Chem. Phys. **116**, 9315 (2002).
[10] D. H. Mordaunt, M. N. R. Ashfold, and R. N. Dixon, J. Chem. Phys. **109**, 7659 (1998).
[11] J. Biesner, L. Schnieder, J. Schmeer, G. Ahlers, X. Xie, K. H. Welge, M. N. R. Ashfold, and R. N. Dixon, J. Chem. Phys. **88**, 3607 (1988).
[12] J. Biesner, L. Schnieder, G. Ahlers, X. Xie, K. H. Welge, M. N. R. Ashfold, and R. N. Dixon, J. Chem. Phys. **91**, 2901 (1989).
[13] L. D. Ziegler, J. Chem. Phys. **82**, 664 (1985).
[14] S. A. Henck, M. A. Mason, W.-B. Yan, K. K. Lehmann, and S. L. Coy, J. Chem. Phys. **102**, 4772 (1995); **102**, 4783 (1995).
[15] A. Nakajima, K. Fuke, K. Tsukamoto, Y. Yoshida, and K. Kaya, J. Phys. Chem. **95**, 571 (1991).
[16] M. Kreglewski, J. Mol. Spectrosc. **72**, 1 (1978).
[17] N. Ohashi and J. T. Hougen, J. Mol. Spectrosc. **121**, 474 (1987).
[18] N. Ohashi, K. Takagi, J. T. Hougen, W. B. Olson, and W. J. Lafferty, J. Mol. Spectrosc. **132**, 242 (1988).
[19] D. Kivelson, J. Chem. Phys. **27**, 353 (1957).
[20] M. Kreglewski, J. Mol. Spectrosc. **133**, 10 (1989).
[21] A. P. Gray and R. C. Lord, J. Chem. Phys. **26**, 690 (1957).
[22] M. Oda, N. Ohashi, and J. T. Hougen, J. Mol. Spectrosc. **142**, 57 (1990), and references therein.
[23] K. Shimoda, T. Nishikawa, and T. Itoh, J. Chem. Phys. **22**, 1456 (1954).
[24] T. Förster and J. C. Jurgens, Z. Phys. Chem. Abt. B **36**, 387 (1937).
[25] E. Tannenbaum, E. M. Coffin, and A. J. Harrison, J. Chem. Phys. **21**, 311 (1953).
[26] M. Tsuboi, A. Y. Hirakawa, and H. Kawashima, J. Mol. Spectrosc. **29**, 216 (1969).
[27] M. Tsuboi and A. Y. Yirakawa, Can. J. Phys. **60**, 844 (1982).
[28] D. P. Taylor and E. R. Bernstein, J. Chem. Phys. **103**, 10453 (1995).
[29] D. P. Taylor, C. F. Dion, and E. R. Bernstein, J. Chem. Phys. **106**, 3512 (1997).
[30] M.-J. Hubin-Franskin, J. Delwiche, A. Giuliani, M.-P. Ska, F. Motte-

Tollet, I. C. Walker, N. J. Mason, J. M. Gingell, and N. C. Jones, J. Chem. Phys. **116**, 9261 (2002).
[31] S. J. Baek, K.-W. Choi, Y. S. Choi, and S. K. Kim, J. Chem. Phys. **117**, 10057 (2002).
[32] P. R. Bunker and P. Jensen, *Molecular Symmetry and Spectroscopy* (NRC Research, Ottawa, 1998).
[33] R. H. Judge and D. J. Clouthier, Comput. Phys. Commun. **135**, 293 (2001).
[34] S. J. Baek, K.-W. Choi, Y. S. Choi, and S. K. Kim, J. Chem. Phys. **118**, 11040 (2003), following paper.
[35] T. J. Sears, P. M. Johnson, and J. BB-Wang, J. Chem. Phys. **111**, 9213 (1999).
[36] P. M. Johnson and T. J. Sears, J. Chem. Phys. **111**, 9222 (1999).